Nanometric positioning accuracy in the presence of pre-sliding and sliding friction: modelling, identification and compensation

Journal:	*Mechanics Based Design of Structures and Machines, An International Journal*
Manuscript ID	LMBD-2015-0183.R2
Manuscript Type:	Research Papers
Date Submitted by the Author:	n/a
Complete List of Authors:	Kamenar, Ervin; University of Rijeka, Faculty of Engineering, Department of Mechanical Engineering Design; University of Rijeka, Centre for Micro and Nano Sciences and Technologies Zelenika, Sasa; University of Rijeka, Faculty of Engineering, Department of Mechanical Engineering Design; University of Rijeka, Centre for Micro and Nano Sciences and Technologies
Keywords:	friction identification and compensation, GMS friction model, self-tuning adaptive PID, nanometric precision and accuracy, handling of microparts

Nanometric positioning accuracy in the presence of pre-sliding and sliding friction: modelling, identification and compensation

Ervin Kamenar [a, †], Saša Zelenika [a]

[a] University of Rijeka – Faculty of Engineering, & Centre for Micro and Nano Sciences and Technologies, Vukovarska 58, 51000 Rijeka, Croatia

Abstract

Pre-sliding and sliding frictional effects, limiting the performances of ultra-high precision mechatronics devices, are studied in this work. The state-of-the-art related to frictional behaviour in both motion regimes is hence considered, and the generalised Maxwell-slip (GMS) friction model is adopted to characterise frictional disturbances present in a micromanipulation device. All the parameters of the model are identified via experimental set-ups and included in the overall MATLAB/SIMULINK model. With the aim of compensating frictional effects, the modelled response of the system is thus compared to experimental results when using proportional-integral-derivative (PID) control, feed-forward model-based compensation and a self-tuning adaptive regulator. The adaptive regulator proves to be the most efficient and is hence used in the final repetitive point-to-point positioning tests allowing to achieve nanometric precision and accuracy.

Keywords: *friction identification and compensation; GMS friction model; self-tuning adaptive PID; nanometric precision and accuracy; handling of microparts*

1 Introduction

Devices characterised by ultra-high positioning precision are often required in precision engineering and microsystems' technologies. In fact, precision mechatronics systems are

† Corresponding author. Tel.: + 385 – (0)51 – 651585; fax: + 385 – (0)51 – 651416; e-mail: ekamenar@riteh.hr

nowadays widely used in machine tools, IT, handling and assembly of MEMS, scientific instrumentation, optical devices, robotics, astrophysics, etc. The interest in ultra-high precision positioning is induced also by the exponential development of the nanotechnologies and their applications (Shore 2010; Schmidt et al. 2014; McKeown and Corbett 2004; Bhushan 2010).

Linear displacements of ultra-high precision mechatronics systems are often achieved by employing sliding and rolling mechanical components, such as ball screws driven by rotary motors and linear guideways. These elements, however, are the main sources of mechanical nonlinearities limiting positioning precision. In ultra-high precision mechatronics devices the dominant disturbance is often friction with its stochastic nonlinear characteristics, which is time-, position- and temperature-dependent. This influences significantly the precision and accuracy of machines by inducing limit cycles around the reference position, stick-slip, static and tracking errors, as well as large settling times (Armstrong-Helouvry et al. 1994; Liu et al. 2013).

In recent literature, frictional behaviour of precision positioning systems is commonly divided into two motion regimes: (gross) sliding (Armstrong-Helouvry et al. 1994; Al-Bender et al. 2004) and pre-sliding displacements (Zelenika and De Bona 2009; Al-Bender et al. 2004; Courtney-Pratt and Eisner 1957). If ultra-high positioning precision and accuracy is aimed for, frictional behaviour has to be properly modelled, identified and compensated for via suitable servo control typologies (Schmidt et al. 2014; Zelenika and De Bona 2009; Hassani et al. 2014).

One axis of a four DOFs ultra-high precision positioning device, to be used for point-to-point positioning in handling and assembly of microparts, is analysed in this work. In section 2 the corresponding set-up and the resulting model are thus described. In section 3 the state-of-the-art concerning the modelling of both pre-sliding and sliding friction is studied. The generalised Maxwell-slip (GMS) integrated friction model (Al-Bender et al. 2004, 2005; Lampaert et al.

2004; Yoon and Trumper 2014) is then adopted to deal with friction of the considered device comprising multiple frictional sources and motion regimes. In section 4 a suitable off-line GMS friction parameter identification method for the elements of the used system is presented. This enables to delineate the overall system model implemented in MATLAB/SIMULINK. The model is proven experimentally to describe excellently the behaviour of the system and thus creates the preconditions to study a way of compensating frictional disturbances. In section 5 positioning performances achieved by using several control schemes aimed at compensating frictional effects are hence investigated and compared to the results of the model. It is therefore shown that a unique reduced-complexity self-tuning adaptive regulator is suitable to achieve high-precision in the presence of both pre-sliding and gross sliding friction. This control algorithm enables therefore in section 6 to adaptively tune in real-time the parameters of the controller so as to compensate the variability of friction in point-to-point positioning. Nanometric precision positioning of the considered system is thus obtained for short (micrometric) and for long (millimetre-range) displacements.

2 Set-up of the high-precision positioning system

The high-precision positioning system considered in this work is a 50 mm translational axis of a four axes mechatronics system to be used for handling and assembly of microparts, which is mounted on a high-stability optical table (Fig. 1). Given its foreseen application, this system is intended mainly for point-to-point positioning and hence its positioning accuracy is more relevant than velocity.

The used actuator is a Faulhaber M1724 006SR DC motor with a nominal voltage $U_N = 6$ V and with dimensions $\phi = 17$ mm, $L = 24$ mm, driven via an inverting TI LM675 analog power amplifier. The motor is coupled with a Faulhaber 15A planetary gearhead with a i = 19:1 reduction ratio. A Heidenhain MT 60K linear incremental encoder with a suitable interpolation unit, allowing a resolution of r_e = 25 nm, is used as a feedback sensor.

The rotation of the actuator is converted to linear displacements via an SKF SH precision rolled ball-screw, having a nominal diameter d_0 = 6 mm and a p = 2 mm pitch. The screw is supported by employing SKF 618/4 ball bearings. The actuator-gearhead assembly is connected to the ball-screw by using a compliant Misumi MCGS13-3-3 coupling.

Translation of the movable part of the considered axis is enabled by using two Schneeberger MINIRAIL profiled miniature MN7 guideways with the overall width and height of, respectively, 8 and 17 mm. Since the movable element supports the remaining axes of the high-precision microparts' manipulation device, the system has to allow ultra-precision positioning of an overall 30 N load.

The data acquisition and control system is based on National Instruments (NI) equipment comprising a reconfigurable PXI-7833R Field-Programmable Gate Array (FPGA) module, a PXI-6221 Data Acquisition Card (DAQ) and a PXI-8196 host computer. The respective control algorithms are programmed as virtual instruments (VIs) in the LabVIEW environment.

A Lasertex LSP 30-3D Michelson-type laser Doppler interferometric system is finally used to assess the achieved positioning accuracy and repeatability. In the specific application, the laser head and the interferometer are mounted on the optical table, while the retroreflector is mounted on the movable part of the device (cf. Fig. 1).

To assess the performances of the system, it is modelled in the MATLAB/SIMULINK software environment. The simplified scheme of the dynamic model is hence shown in Fig. 2 where the interconnection of all the electromechanical elements (indicated in bold), with their main physical characteristics, is depicted. The typical electromechanical dynamics of the DC actuator is inducing here, via the gearhead, a rotation φ_r of the ball-screw characterised by its pitch p. The reduction ratios of the gearhead and the ball-screw are duly taken into account. Rotation φ_r is hence converted, taking into account the stiffness and damping effects of the elements of the system, into a linear displacement x_{stage} of the translator bearing the movable load of mass m. The frictional effects of the rotational elements M_f and of the translating elements F_f are considered as disturbances whose model is to be determined so as to enable their compensation via a suitable controller. The achieved position x_{eff} is finally validated via interferometric measurements.

3 Friction modelling

As already evidenced in the introduction, the effects of friction hindering precision positioning are conventionally considered with their properties related to the sliding and the pre-sliding regimes of motion.

3.1 Sliding behaviour

Following the pioneering work on friction of da Vinci, Amontons, Euler, Coulomb, Newton and Reynolds, at the beginning of the 20th century Stribeck introduced the nowadays widely used Stribeck friction curve. As depicted in Fig. 3a, the friction force F_f along this curve is dependent on velocity only and encompasses all the macro-dynamic frictional effects (Armstrong-Helouvry et al. 1994):

- static friction F_s,
- velocity weakening between static and kinetic friction (often labelled: “Stribeck effect”),
- Coulomb friction F_C

- and viscous friction.

3.2 Pre-sliding behaviour

The conventional Stribeck friction model does not allow to address properly the frictional discontinuity at zero (or almost-zero) velocity, i.e. it does not take into due consideration position-dependent frictional effects at the micro-scale. These effects, although being qualitatively repeatable, quantitatively depend on complex interactions between contacting surfaces (Courtney-Pratt and Eisner 1957; Al-Bender et al. 2004). A pioneering work in this field is that of Courtney-Pratt and Eisner (1956) that, based on experimental observations, determined that pre-sliding is an elasto-plastic nonlinear effect with hysteretic contributions that depends on normal and tangential forces as well as on the history of motion. This nonlinear effect is characterised with a spring-like behaviour with multiple stiffnesses comprising plasticity and damping. It encompasses displacements that can amount up to some hundred micrometres and can thus have a significant detrimental effect in ultra-high precision devices.

The effect can be modelled only via complex empirical models (Armstrong-Helouvry et al. 1994; Al-Bender et al. 2004; Hsieh and Pan 2000). What is more, pre-sliding hysteresis is characterised by *non-local memory* i.e., as shown in Fig. 3b, an input-output relationship such that, when there are multiple displacement reversals, at each closure of the inner loop, the curve of the outer loop is followed again (Swevers et al. 2000; Al-Bender et al. 2004).

3.3 Friction models

Based on the above and other subsequent studies of pre-sliding, and motivated by the need for fast and accurate positioning, several integrative heuristic grey-box friction models (Worden et al. 2007), based on rate-state phenomenology, have recently been proposed. Most of them stem from *Dahl's model* (Dahl 1968) that accounts for Coulomb friction and the hysteretic pre-sliding displacement with a smooth transition around zero velocity. However, Dahl's model does not embody frictional lag, non-local memory or the Stribeck effect and it cannot predict stick-slip. These shortcomings are partly addresses by the *LuGre friction model*. In this case, Dahl's static differential equation is developed into a dynamic state equation – with the state corresponding to the average deformation of surface asperities (modelled as bristles) and the inclusion of the Stribeck effect (Canudas De Wit et al. 1995). In the LuGre model, a smooth transition between pre-sliding and gross sliding is assured without the need of a switching function (Wu et al., 2014). Moreover, the model includes *frictional lag* (or *frictional memory*), i.e. a hysteretic effect that results in friction forces higher for accelerating slippage than for decelerating motion (Al-Bender et al. 2004). The model encompasses also *rising static friction*, i.e. the variability of the value of the breakaway force depending on dwell time, as well as stick-slip. It cannot still, however, take into account the hysteretic behaviour with non-local memory (Swevers et al. 2000; Al-Bender et al. 2005).

With the aim of representing non-local memory, albeit at the expense of difficult implementation in real-time control, the *Leuven friction model* (Swevers et al. 2000) adds to the LuGre model a hysteresis function implemented via memory stacks, i.e. via Maxwell-slip elements. Concurrently with the Leuven model, Hsieh and Pan (2000) developed a comprehensive *model of pre-sliding friction* combining plastic deformation with creep and work hardening and, in a series connection, nonlinear elastic deformation with memory and wipe-out effects, in parallel with a viscous damper. This model is qualitative and difficult to implement due to a large number of parameters that are physically hard to interpret and have to be empirically identified via cumbersome tests.

Most of the evidenced shortcomings are avoided by using the recently proposed grey-box physical *generalised Maxwell-slip* (GMS) model, whose computational implementation in real-time control is simple as it is based on a small number of easily identifiable parameters. The model has been proven to describe with high fidelity frictional phenomena observed experimentally and allows both the pre-sliding and sliding regimes to be modelled by a continuous friction force function. GMS is based on a parallel connection of N massless (phenomenological) elementary Maxwell elasto-slip blocks having all the same input – velocity v, and one output – the friction force F_i acting on the i-th block (Fig. 4a). In pre-sliding motion, velocity v is the derivative of the state variable z, which represents the average deflection of surface asperities (Al-Bender et al. 2004, 2005; Lampaert et al. 2004; Yoon and Trumper 2014). Two states of either rate-independent hysteresis with non-local memory in pre-sliding, or of (steady-state) slip with frictional lag, determine the behaviour of each block depending on W_i – the weighted Stribeck curve for each block (Lampaert et al. 2004; Yoon and Trumper 2014):

$$W_i = \alpha_i \cdot s(v) \tag{1}$$

Here $s(v)$ designates a velocity weakening curve that is bounded by F_s and F_C and depends on the direction of motion:

$$s(v) = \mathrm{sgn}(v) \cdot \left[F_C + (F_s - F_C) \cdot e^{-\left(\frac{|v|}{V_S}\right)^{\delta}} \right] \tag{2}$$

V_S indicates the Stribeck velocity, whereas δ is the Stribeck curve shape factor. α_i is, in turn, the relative weight of each Maxwell block defined by its stiffness k_i. This parameter is determined by the piecewise approximation of the experimentally assessed pre-sliding behaviour, with respect to the integral effect of all Maxwell-slip blocks connected in parallel (Fig. 4b):

$$k_i = \frac{\Delta F_i}{D_i} \tag{3}$$

$$\alpha_i = \frac{k_i \cdot D_i}{F_s} \tag{4}$$

Conditions (3) and (4) imply that the sum of all contributions α_i adds up to 1:

$$\sum_{i=1}^{N} \alpha_i = 1 \tag{5}$$

In the above equations one common form of the velocity weakening curve is assumed for all the blocks, which allows reducing the number of unknown parameters. It can thus be shown that as few as four Maxwell elements can provide a very good fit to experimental data (Al-Bender et al. 2005; Tjahjowidodo et al. 2005). The state of motion of each block will hence be determined based on the condition:

- if $|F_i(v)| < |W_i(v)|$ the block sticks

$$\frac{\mathrm{d}F_i}{\mathrm{d}t} = k_i \cdot v \tag{6}$$

- else: the block slips

$$\frac{\mathrm{d}F_i}{\mathrm{d}t} = \mathrm{sgn}(v) \cdot C \cdot \left(\alpha_i - \frac{F_i}{s(v)}\right) \tag{7}$$

C is the attraction parameter indicating how fast slipping dynamics follows the velocity weakening curve.

The total friction force F_f affecting the system will hence be the sum of the forces (outputs) of all the N Maxwell blocks with the addition of a viscous term:

$$F_f = \sum_{i=1}^{N} F_i\,(t) + \sigma \cdot v(t) \tag{8}$$

where σ is the viscous friction coefficient.

Due to its comprehensiveness and simplicity, the GMS friction model enables the study of frictional disturbances on the behaviour of the system and hence the application of control schemes that are suitable to achieve ultra-high precision positioning. So far, however, the GMS model was applied merely to compare the behaviour of different friction models, to identify the model parameters or to verify the response of rudimental (often bulky) mechanical systems in limited motion ranges, with limited accuracies and/or with very specific actuating signals (Tjahjowidodo et al. 2005; Lampaert et al. 2004; Al-Bender et al. 2004; Yoon and Trumper 2014). The GMS model will, in turn, be used in this work to model the friction effects in the ultra-high precision mechatronics system aimed at nanometric positioning where the system is characterised by multiple frictional sources (cf. Fig. 2) and some of the elements of the system can be in the sliding motion regime while others are still in pre-sliding. To achieve this ambitious goal, the parameters of the GMS friction model have to be identified off-line first.

4 Identification of GMS friction model parameters

As indicated in Fig. 2, the friction parameters are experimentally assessed separately for the DC actuator-gearhead assembly and for the stage.

4.1 Friction parameters of the DC actuator-gearhead assembly

The friction in the actuator-gearhead assembly is induced by the brushes-commutator contacts, the radial bearings, the point contacts of gears' teeth as well as the velocity dependent viscous effect (Zelenika and De Bona 2009). In order to determine the pre-sliding behaviour, a suitable experimental set-up, coupling the actuator-gearhead assembly to a Baumer rotational incremental encoder via a 3D printed ABS frame, is used. By employing an interpolation unit, the resolution of the encoder is increased from 12 bits by 400 times, resulting in a 3.8 μrad resolution.

The voltage signal on the analog output of the used NI DAQ card is thus slowly ramped and fed, via the power amplifier, to the actuator (cf. section 2). The small voltage drop on a shunt resistor, connected in series with the actuator, is scaled up by using a custom-designed low-noise instrumentation amplifier and fed into the DAQ card. The actual value of the stationary voltage input is, in turn, used to calculate the current. Finally, considering that in the used configuration the inertial effects and damping are negligible, friction torque M_f is obtained by multiplying the current with the torque constant $k_M = 6.59$ mNm/A of the actuator, while rotation is simultaneously measured via the encoder connected to the digital inputs of the FPGA module.

The average obtained results, with the respective deviations in repetitive measurements, are reported in Fig. 5a. It can thus be observed that a typical nonlinear pre-sliding behaviour, as shown in Fig. 4b, is obtained and is characterised by a large time and position variability. Frictional torques M_{fpr} with average values of up to 200 μNm and respective rotations at the output of the gearhead φ_r of up to ca. 7 mrad are obtained.

The same measurement set-up is used to assess the behaviour of the actuator-gearhead assembly in the sliding regime as well. The angular velocity ω_r of the steady state rotation at the output of the gearhead is hence calculated as the derivative of the readings of the encoder and is validated also from the input voltage U as:

$$\omega_r = \frac{U - I \cdot R}{i \cdot K_E} \tag{9}$$

where I, $R = 3.41\ \Omega$ and $K_E = 0.69$ mV/min^{-1} are, respectively, the current absorbed by the motor, the resistance on its terminals and its back EMF (electro-magnetic force) constant, while i is the gearhead reduction ratio. For this purpose, a further analog input of the DAQ card is used to measure the voltage.

Closed loop experiments with velocity proportional-integral (PI) control are hence performed at constant velocities in the ω_r = 0 to ± 16 rad/s range. The friction vs. velocity dependence is obtained by averaging a large number of measurements. The resulting frictional torque in the sliding regime M_{fsl} vs. ω_r is hence shown in Fig. 5b, where the expected Stribeck curve is clearly visible. The marked viscous friction component is mainly due to the influence of the back EMF effect (Zelenika and De Bona 2009). To enhance the clarity of the figure, the dispersion from average values, roughly ± 6 % for lower angular velocities and up to ± 15 % for larger velocities, is not shown. A careful examination of Fig. 5b allows noticing a certain asymmetry depending on the direction of motion. All these facts confirm hence the marked stochastic nature of frictional effects in both pre-sliding and sliding motion.

The data of Fig. 5 can also be used to determine the parameters of the Maxwell-slip blocks of the GMS model. Referring to Fig. 4 and Equations (3) and (4), the characteristic parameters of the Maxwell blocks, determined from the data of Fig. 5a, are reported in Table 1. Considering the suggestions given in Al-Bender et al. (2005), as well as the resulting computational complexity, six blocks are considered sufficient.

In a first approximation, the attraction parameter C of the GMS model can be obtained as the inverse value of the Stribeck velocity ω_S (Jamaludin 2008) – refer to Table 2. In order to confirm this assumption, repetitive experiments, while the actuator-gearhead assembly is accelerated and decelerated, are conducted. By comparing the obtained results with those from the MATLAB/SIMULINK model, it is confirmed that a change of the value of C has no major impact on system's response. It is also to be noted that in point-to-point positioning the velocity and the acceleration are low and there are no sudden dynamic and/or periodic effects that would induce frictional lag (Al-Bender et al. 2004, 2005). In a first instance, the value of C in the considered low-dynamics conditions is thus set to 1.

The remaining parameters of the GMS model, relative to its transition from pre-sliding to sliding and then in the sliding regime itself, are determined from the measurements reported in Fig. 5b.

With analogy to Equation (2) and considering the influence of viscous friction, the Stribeck frictional behaviour can hence be modelled as:

$$M_{fsl} = \left[M_C + (M_s - M_C) \cdot e^{-\left(\frac{|\omega_r|}{\omega_S}\right)^{\delta}} \right] + \sigma \cdot \omega_r \tag{10}$$

where M_s and M_C are the static and Coulomb frictional toques, ω_s is the Stribeck angular velocity, while the other designations are the same as in the above expressions. The measured data are fit to the Stribeck curve of equation (10) by using the *lsqcurvefit* function of the MATLAB Optimization Toolbox. Since there is an asymmetry of the frictional behaviour depending on the direction of motion, two sets of characteristic parameters are obtained. However, since the difference of the values of the same parameter, depending on direction, is smaller than the variability of frictional parameters, a single set of nominal parameters can be adopted (Table 2). The GMS model of the actuator-gearhead assembly is therefore fully defined.

4.2 Friction parameters of the linear guideways

To assess the pre-sliding frictional behaviour of the linear guideways, an elaborated experimental set-up is conceived (Fig. 6). Tangential loading is hereby applied by using a micro-tensile machine equipped with a 1 kN load cell allowing load increments with a 10 mN resolution. An incremental increase of the load is transmitted to the movable parts mounted on the optical bench via a pulley and a carbon-based fibre. Load increments are made when the system comes to an almost complete rest, since displacement on the nanometric level can be observed even after extended time periods (Zelenika and De Bona 2009). The resulting displacements are measured via the interferometric system. In order to validate the position and time variability of the measured effects, more than 50 experiments are conducted using different starting points in various periods during the day.

The obtained results are depicted in Fig. 7. The typical nonlinear elasto-plastic pre-sliding behaviour with non-local memory can hence be observed (Fig. 7a). The narrow loops, obtained by reducing the tangential forces and increasing them again, allow evidencing that the elastic component of the overall behaviour is rather small, i.e. that it is essentially irreversible, whereas the slope (i.e. stiffness) of the elastic component is almost constant irrespective of the position on the curve where the return loop is started. The average overall pre-sliding behaviour is displayed for frictional forces F_{fpr} of up to about 0.9 N and respective displacements x of up to roughly 40 μm. It can, however, be observed (Fig. 7b) that these values have a conspicuous variability depending on the point of the stage where the measurement is performed. A large dispersion (up to about ± 15 %) in repetitive measurements is also evident, which is partly due to temperature variations and partly to differing dwell times inducing the mentioned rising static friction effect and is often encountered in ball-bearing stages.

The experimental data of the frictional behaviour of the linear guideways can again be used to determine the parameters of the Maxwell blocks of the GMS model. Six Maxwell blocks are considered again, and their characteristic stiffness and relative weights are reported in Table 3. The response of the MATLAB/SIMULINK model corresponding to this data, reported also in Fig. 7b, confirms the validity of the determined parameters and of the model itself.

It is to be noted here in particular that, due to the reduction ratios of the gearhead and the ball-screw (cf. also Fig. 2), the frictional effect of the mechanical parts of the system, when reduced to the motor shaft, will amount to a frictional torque comparable to the variability of friction present in the actuator-gearhead assembly. This consideration, proven by experimental measurement on the whole system as well, confirms that the biggest frictional contribution will be that of the actuator. Moreover, due to the reduction ratios, even when the motor-gearhead assembly overcomes sticktion and enters sliding, the mechanical transmission elements will still be in pre-sliding. Most significantly, ultra-high precision positioning will certainly happen when the linear slide will be in the pre-sliding regime (Zelenika and De Bona 2009). All this implies that only the pre-sliding frictional behaviour of the linear guideways is to be considered in the quest for attaining ultra-high precision, validating further the assumption that the attraction parameter C of the GMS model has lower relevance. Moreover, given its magnitude, in the development of a suitable controller, this behaviour can be considered as a perturbation to the markedly stochastic frictional effects and can hence be compensated, as it will be practically shown, by using an appropriate adaptive control typology (Armstrong-Helouvry et al. 1994; Astrom and Hagglund 1995).

5 Compensation of the disturbances induced by friction

As already stated, ultra-high positioning precision in the presence of friction can generally be achieved only by using servo control. Results obtained from the MATLAB/SIMULINK model are thus compared in this part of the work to experimental results attained by employing different control typologies. In all the considered cases, the aim of avoiding the need to use complex controllers that would be separately applied in the pre-sliding and in the sliding regime (“dual-mode controllers”), with the respective switching schemes, is achieved, i.e. a single control typology is used in the whole motion range.

5.1 PID control without specific friction compensation

PID controllers use in the feedback loop proportional (K_P), integral (K_I) and derivative (K_D) terms (i.e. PID gains) that multiply the error determined by the feedback sensor (Armstrong-

Helouvry et al. 1994) – framed detail in Fig. 8. A discrete form of the PID controller is implemented in this work on the FPGA module with a sampling time of T = 100 μs that is chosen so as to assure that even during the rise time the sampling period is approximately 10 times larger than the closed loop system bandwidth. By approximating the integral and the derivative terms using a backward differences algorithm (Astrom and Hagglund 1995), the output of the PID controller $U_c(n)$ (cf. also Fig. 2) can thus be defined as:

$$U_c(n) = \mathrm{K_P} \cdot e(n) + \mathrm{K_I} \cdot \sum_{k=1}^{n} e(k) + \mathrm{K_D} \cdot \left[x_{stage}(n) - x_{stage}(n-1)\right] \tag{11}$$

where $e(n)$ is the discrete error term, $e(k)$ is the integral error term, k is the summation variable for the integral term, n is the discrete time step and $x_{stage}(n)$ and $x_{stage}(n–1)$ are the measured positions in two subsequent time steps. The integral and derivative gains are calculated based on the signal sampling period T, as well as the integral and derivate time constants T_I and T_D, as:

$$\mathrm{K_I} = \frac{\mathrm{K_P} \cdot T}{T_I}, \quad \mathrm{K_D} = \frac{\mathrm{K_P} \cdot T_D}{T} \tag{12}$$

The tuning of the PID gains is conducted in two steps: the user-friendly time-domain Ziegler-Nichols method is used to achieve a rough estimate of the gains, whereas fine-tuning is performed experimentally. The obtained gain values are used to assess via the MATLAB model the stability of the system proving that in all the considered cases a positive phase margin of at least 30° and a gain margin of about 40 dB are obtained.

5.2 PID control with feed-forward compensation

As suggested in (Swevers et al. 2000; Lampaert et al. 2004; Tjahjowidodo et al. 2005; Yoon and Trumper 2014; Hassani et al. 2014), the nonlinear stochastic effects related to friction can be compensated by including the suitable disturbance values in a feed-forward control scheme (Fig. 8). In this case, the disturbances are, obviously, based on the GMS friction model of the actuator-gearhead assembly and of the linear guideways with the values of the characteristic parameters determined in section 4.

Although being model-based, when considering the overall system structure, this approach can be computationally complex. In addition, in the considered set-up it is based on the nominal values of the velocity of the mechatronics system. In fact, when coupled with all VIs needed to process the input and output signals of system's components, the algorithm needed to determine the actual velocity of the linear stage by differentiating its measured position, gives rise to overloading problems related to the limited number of programmable logic blocks available in the FPGA module. When, in turn, the differentiation algorithm is implemented as a LabVIEW Host VI, the reachable sampling time (in the ms range) limits the positioning performances of the used device.

5.3 Self-tuning adaptive PID regulator

In the set of available adaptive nonlinear control schemes, self-tuning regulators (STR) are the best suited for settings with stochastic changes in the system to be controlled on-line in digital closed-loop environments, as it is flexible and computationally easy to implement (Fig. 9a) (Astrom and Hagglund 1995). An STR adaptive PID control scheme, originally proposed by Lin and co-authors (2000), is therefore used to adaptively control the described mechatronics system. In the herein considered case, the objective function of adaptive tuning is minimising positioning error e with respect to the reference position x_{ref}:

$$e = x_{ref} - x_{stage} \tag{13}$$

The adaptation of the PID gains is hence achieved on-line, thus allowing the probabilistic changes of frictional effects and other eventual external disturbances to be effectively compensated, resulting effectively in a black-box model (Worden et al. 2007). As depicted in Fig. 9b, the resulting STR adaptive PID regulator is hence constituted by four subsystems: one for each of the PID gains and one encompassing the considered positioning system itself. The tuning of PID gains to adapt the response of the system to the variation of its parameters, including those related to friction, is in turn based on the theory of adaptive interactions (Lin et al. 2000). The implementation of the tuning algorithm is quite straightforward since, in the simplified form, the dependence on the plant model can be eliminated, whereas the adaptation of the parameters of the regulator is reduced to an algorithm based on a single adaptation coefficient γ and the outputs y_i of the considered subsystems (Lin et al. 2000). It was shown that this simplified scheme is stable and converges quickly for linear and nonlinear systems, as well as with or without noise and/or time-delays. What is more, this scheme does not require an intricate computational implementation of the frictional model, since the adaptation of the PID gains compensates effectively all the dynamic changes (Lin et al. 2000). This implies that the controller scheme, in contrast to the considered feed-forward scheme, can be efficiently implemented even when large parts of the computational capacities are devoted to real-time monitoring of the effective velocity of the system (within the sampling time of 100 μs).

5.4 Results and discussion

In a first instance, the response of the used mechatronics system to sinusoidal excitations of varying amplitudes in the range from 1 μm to 1 mm is performed. The results obtained via the MATLAB model and by practically employing the considered control typologies are shown as tracking errors Δ_t with respect to the input signal.

As depicted in Fig. 10 for a sinusoidal signal with a 10 μm amplitude at a 0.03 Hz frequency, results obtained by using PID control (black solid line) induce significant differences between the time-variant nominal (i.e. input) position and the actual response of the system x_{stage} as measured via the Heidenhain encoder. As expected, the PID gains optimised for a certain motion range, do not allow achieving similar accuracies for different motion amplitudes (Armstrong-Helouvry et al. 1994). Iterative repetitive optimisation of the PID gains according to the outlined procedure is hence needed for each motion amplitude or, in the case of random motion amplitudes, the gains would have to be adaptively tuned. For the same reason, the PID gains determined for one position on the linear guideways can prove to be not optimal even for the same motion amplitude at a different point along the stage and/or in different time or temperature conditions.

Results obtained by using the respective MATLAB model of Fig. 2 with the experimentally determined PID gains, are also shown in the figure (circular markers). It can thus be seen that the model describes very reliably the physics of the system although, obviously, not allowing to capture the effects induced by the stochastic variability of friction. All these facts confirm thus the need to resort to more elaborated control typologies.

When PID control is complemented with an additional feed-forward compensator based on the determined GMS friction parameters (grey solid line in Fig. 10), the tracking performance improves significantly, resulting in tracking errors limited to less than ± 500 nm. Obviously, the stochastic variability of frictional effects is not taken into account in this case either. Despite this fact, this control configuration allows achieving good results for varying motion amplitudes and positions along the stage, albeit at the expense of computational complexity and the need to perform slower motions evidenced above. In this respect, it should be considered also that, as mentioned before, due to the effect of speed ratios, the influence of pre-sliding friction of the linear guideways in fine positioning corresponds to a negligible virtual variation of sliding friction occurring concurrently on the actuator-gearhead assembly. This, in turn, implies that the burdensome determination of the pre-sliding friction parameters can be avoided altogether (Zelenika and De Bona 2009). In the case of the same regulator used in the MATLAB model (diamond-shaped markers in Fig. 10), the feed-forward friction predictor basically cancels the supposedly invariant effects of frictional disturbances, inducing thus a response with very small tracking errors.

Finally, by using the STR adaptive PID controller (dotted line in Fig. 10), in all the considered cases excellent positioning accuracies (± 150 nm), limited basically by the limitations of the PID controller at velocity reversals, by the time constants of the used electrical elements and by the measurement uncertainty of the feedback sensor, are achieved rapidly and reliably. In fact, by tuning via the MATLAB model the values of the adaptation parameter γ so that the resulting PID gains never approach the values leading to a possible occurrence of instabilities (cf. also section 5.1), the used simplified STR algorithm allows fast convergence to high-accuracy tracking conditions. The regulator hence compensates efficiently the variabilities of frictional effects, despite the fact that it is basically a black-box model not relying on a physical model of friction. The high potential of this control typology is further confirmed by the fact that the MATLAB model of the system, regulated with the STR regulator, results in very small tracking errors (dashed line in Fig. 10).

6 Ultra-high precision positioning of the considered set-up

Considering the results reported in section 5, and given that the aim of the work is achieving ultra-high precision point-to-point positioning applied to handling and assembly of microparts, the STR adaptive controller is finally used to repetitively position the used device. The mechatronics system performs thus in each move a displacement from an initial to the reference position. The interferometric system of section 2 is used to validate externally x_{stage} as measured by the encoder, i.e. to assess the achieved unidirectional positioning accuracies and repeatabilities while each x_{eff} measurement is repeated 10 times (cf. Figures 1 and 2). The uncertainty of the interferometric measurements, performing a careful iterative mounting and alignment of the system and measuring and compensating in real-time for the atmospheric changes, is estimated to be limited to ± 40 nm.

Results in terms of the reached x_{stage} positions as measured by the Heidenhain encoder, are depicted in Fig. 11 for short-range (micrometric – left ordinate of Fig. 11) and long-range (millimetre-range – right vertical axis in Fig. 11) motions. It is to be noted once more that short-range positioning implies that the linear stage is in the pre-sliding motion regime in the whole travel range (cf. Fig. 7), although the actuating elements are already sliding (cf. Fig. 5). For long-range travels, the whole system is in turn in sliding motion during the approach to the reference position and then switches to the pre-sliding regime of the linear stage during the settling to the final position.

In Fig. 11 are reported also the results obtained by using the MATLAB/SIMULINK model of Fig. 2 with the GMS friction parameters determined in section 4. It is hence evident that the adaptive nature of the used controller allows compensating efficiently all the present mechanical nonlinearities and their variabilities, permitting in all the considered cases to achieve nanometric positioning precision. It is, in fact, evident that in all the considered cases the reference positions are reached. The resulting error in the MATLAB model is hence negligible, confirming its excellent physical foundation, while in the case of experimental measurements, precision and accuracy comparable to the resolution of the used feedback sensor are always obtained.

The correspondingly achieved performances in terms of unidirectional accuracy and repeatability, as measured independently by the interferometric system, are shown in Table 4. These values are calculated, in the absence of specialised microparts standards, according to the ISO 230-2:2014 machine tools' standard that defines them basically to be equal to $4 \cdot s$ (s being the standard deviation of repetitive measurements). It is hence established that in all the considered cases the achieved precision and accuracy are better than 250 nm, i.e. that the stochastic frictional disturbances are successfully compensated.

7 Conclusions and outlook

In this work one axis of a multi-DOFs micropositioning mechatronics system aimed at handling and positioning of microparts is conceived, designed and set-up. The pre-sliding and sliding stochastic nonlinear frictional effects present in the system, which limit its positioning precision, are hence thoroughly studied, modelled and identified via elaborated experimental set-ups. The devised procedure of identifying the friction parameters allows hence establishing that, due to reduction ratios, the frictional contribution of the actuator-gearhead assembly is the most significant one and that, even when this assembly enters the sliding motion regime, the downstream elements will still be in pre-sliding. The identification of friction parameters enables also to study different compensation approaches. It could therefore be shown that, by implementing a unique, simple and reliable STR adaptive PID control scheme, the stochastic nonlinear frictional disturbances can be efficiently compensated. Closed-loop ultra-high precision positioning is therefore obtained. In fact, in all the considered short-range (where the overall motion is in the pre-sliding regime) and long-range (where the system undergoes both sliding and pre-sliding frictional effects) unidirectional point-to-point experimental positioning steps, precision and accuracy limited only by the resolution of the used feedback sensor are obtained. A further external assessment employing a laser interferometer allows establishing that positioning accuracy and repeatability better than 250 nm are always obtained.

In future work, the authors plan to investigate the possibility to use even more elaborated control typologies based on a direct adaptive compensation of the variability of the observer-based frictional parameters. In this case, suitable real-time metrics enabling to discriminate the influence of the various frictional effects would also have to be developed. Other types of actuators (e.g. stepper motors, voice-coils) and of feedback transducers (e.g. LVDT), will also be considered. Finally, the full operability of the multi-axes micropositioning systems will be tested and applied to handling of microparts. Further applications in machine tools, metrology, optical systems or scientific instrumentation will also be investigated.

Acknowledgements

This work was made possible by using the equipment funded via the EU European Regional Development Fund project no. RC.2.2.06-0001: “Research Infrastructure for Campus-based Laboratories at the University of Rijeka”.

References

Al-Bender, F., Lampaert, V., Swevers, J. (2004). Modeling of dry sliding friction dynamics: From heuristic models to physically motivated models and back. *Chaos* 14(2):446-460.

Al-Bender, F., Lampaert, V., Swevers, J. (2005). The Generalized Maxwell-Slip Model: A Novel Model for Friction Simulation and Compensation. *IEEE T Automat Contr* 50(11):1883-1887.

Armstrong-Helouvry, B., Dupont, P., Canudas de Wit, C. (1994). A Survey of models, analysis tools and compensation methods for the control of machines with friction. *Automatica* 30(7):1083-1138.

Astrom, K. J., Hagglund, T. (1995). *PID Controllers: Theory, Design and Tuning* (2nd ed.). Research Triangle Park: Instrument Society of America.

Bhushan, B. (ed.). (2010). *Springer Handbook of Nanotechnology* (3rd ed.). Berlin: Springer.

Canudas De Wit, C., Olsson, H., Astrom, K. J., Lischinsky, P. (1995). A New Model for Control of Systems with Friction. *IEEE T Automat Contr* 40(3):419-425.

Courtney-Pratt, J. S., Eisner, E. (1957). The effect of a tangential force on the contact of metallic bodies. *Proc Roy Soc Lond A Mat* 238(1215):529-550.

Dahl, P.R. (1968). A solid friction model. Technical report. Aerospace Corporation.

Hassani, V., Tjahjowidodo, T., Do, T. N. (2014). A survey on hysteresis modeling, identification and control. *Mech Syst Signal Pr* 49(1–2):209-233.

Hsieh, Ch., Pan, Y. C. (2000). Dynamic behavior and modelling of the pre-sliding static friction. *Wear* 242(1–2):1-17.

Jamaludin, Z. (2008). Disturbance Compensation for Machine Tools with Linear Motor Drives. Doctoral thesis, Katholieke Universiteit, Leuven, Belgium.

Lampaert, V., Swevers, J., Al-Bender, F. (2004). Comparison of model and non-model based friction compensation techniques in the neighbourhood of pre-sliding friction. In *Proc American Control Conf* vol 2. (pp. 1121-1126). Boston, USA.

Lin, F., Brandt, R. D., Saikalis, G. (2000). Self-Tuning of PID controllers by adaptive interaction. In: *Proc Am Contr Conf* vol 5. (pp. 3676-3681). Chicago, USA.

Liu, L., Wu, Z., Liu, H. (2013). Modeling and Analysis of the Crossfeed Servo System of a Heavy-Duty Lathe with Friction. *Mech Based Des Struc* 41(1):1-20.

McKeown, P., Corbett, J. (2004). Ultra Precision Machine Tools, In Klocke, F., Pritschow, G., eds. *Autonome Produktion*, Berlin: Springer, 313-327.

Schmidt, R. M., Schitter G., Rankers A., van Eijk J. (2014). *The Design of High Performance Mechatronics – High-tech Functionality by Multidisciplinary System Integration* (2nd ed.). Delft: U Press.

Shore, P. (2010). Precision engineering for astronomy and gravity science. *CIRP Ann-Manuf Techn* 59(2):694-716.

Swevers, J., Al-Bender, F., Ganseman, C. G., Projogo, T. (2000). An Integrated Friction Model Structure with Improved Presliding Behavior for Accurate Friction Compensation. *IEEE T Automat Contr* 45(4):675-686.

Tjahjowidodo, T., Al-Bender, F., Van Brussel, H. (2005). Friction Identification and Compensation in a DC Motor. In: *Proc 16th IFAC World Cong*. (paper 4017). Prague, CZ.

Worden, K., Wong, C. X., Parlitz, U., Hornstein, A., Engster, D., Tjahjowidodo, T., et al. (2007). Identification of pre-sliding and sliding friction dynamics: Grey box and black-box models. *Mech Sys & Sign Processing* 21:514-534.

Wu, Z. Y., Dowell E. H., Tang D. M. (2014) Damping Analysis In Beams Subject To Presliding Friction. *Mech Based Des Struc* 42(2):229-243.

Yoon, J. Y., Trumper, D. L. (2014). Friction modeling, identification, and compensation based on friction hysteresis and Dahl resonance. *Mechatronics* 24(6):734-741.

Zelenika, S., De Bona, F. (2009). Nano-positioning using an adaptive pulse width approach. *Proc Inst Mech Eng* 223(C8):1955-1963.

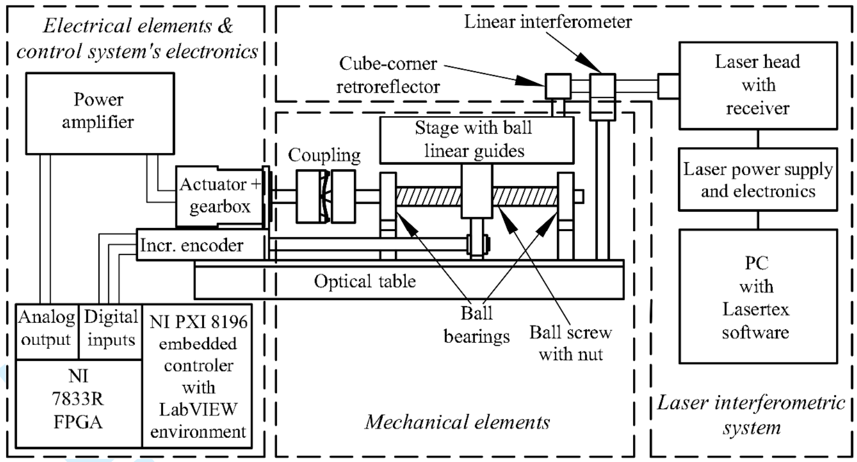

Fig. 1 Scheme of considered ultra-high precision positioning system

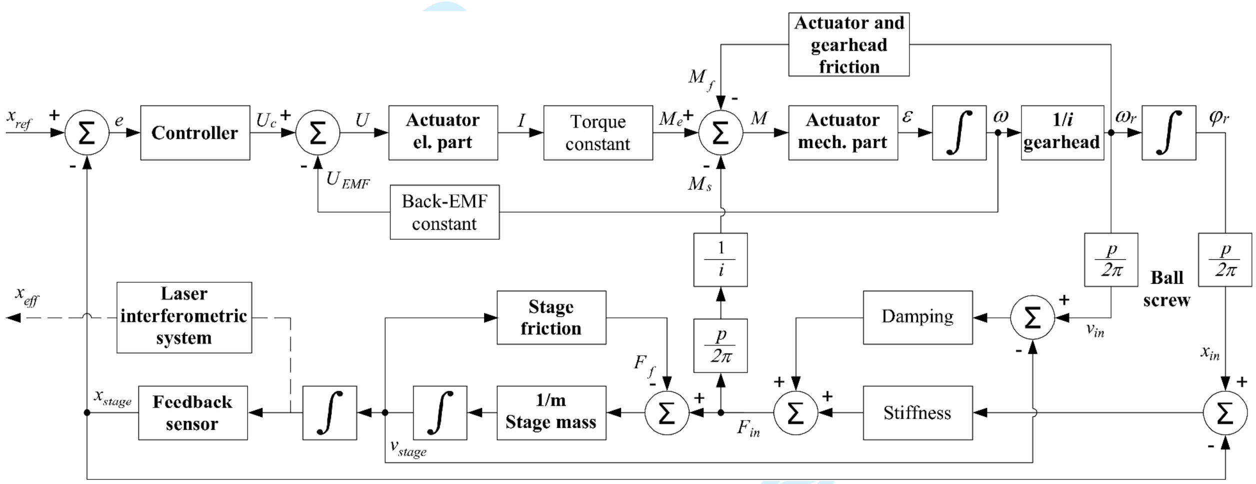

Fig. 2 Model of considered ultra-high precision mechatronics system

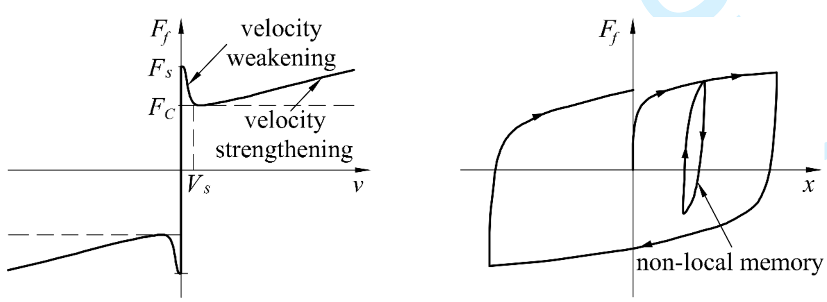

(a) (b)

Fig 3 Stribeck curve in gross sliding (a) and hysteretic frictional behaviour in pre-sliding with non-local memory (b)

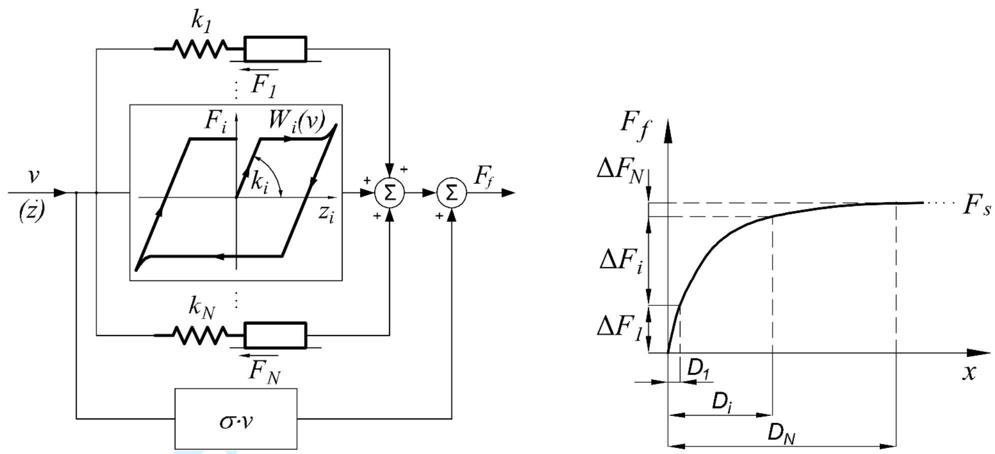

(a) (b)

Fig. 4 Scheme of the Maxwell-slip blocks (a) and respective variables of the GMS model (b)

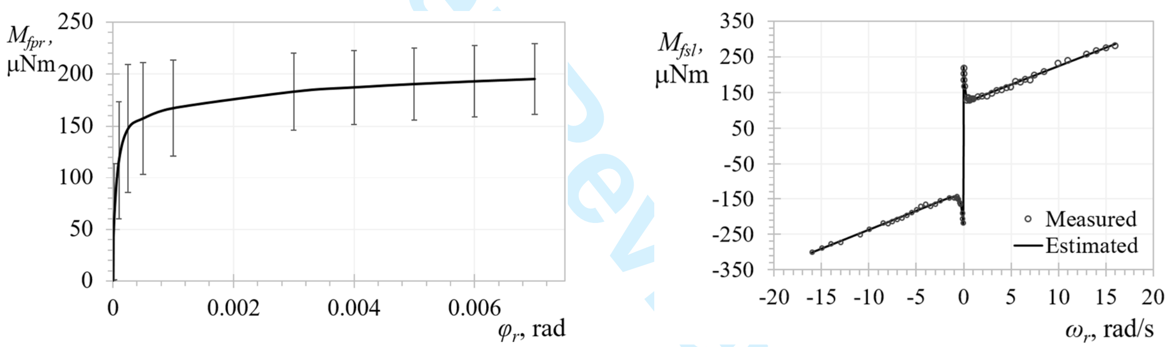

(a) (b)

Fig. 5 Friction torque of the actuator-gearhead assembly in the pre-sliding (a) and in the sliding (b) regime

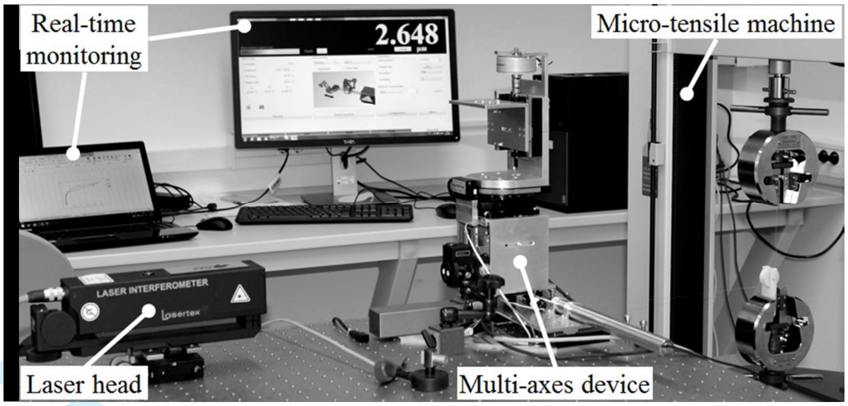

Fig. 6 Set-up for the measurement of the pre-sliding behaviour of the linear guideways

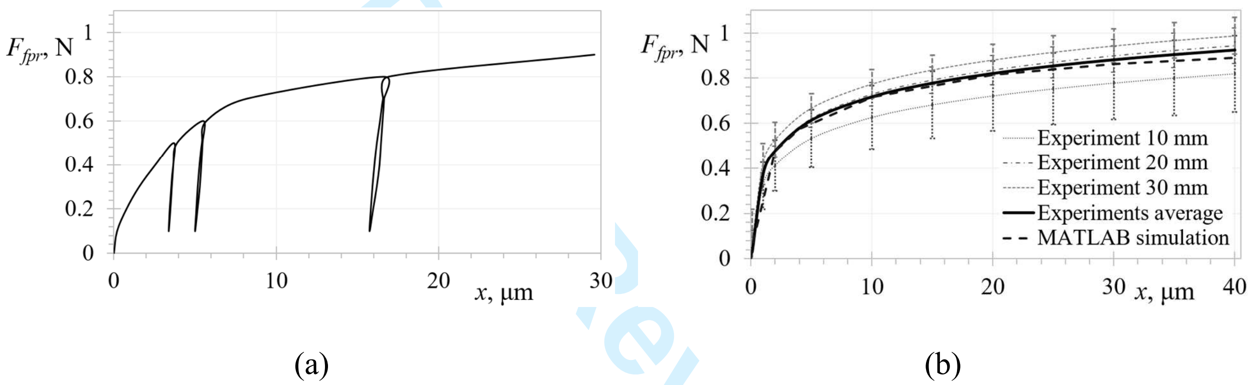

Fig. 7 Pre-sliding friction of linear guideways (a) and variability in repetitive measurements (b)

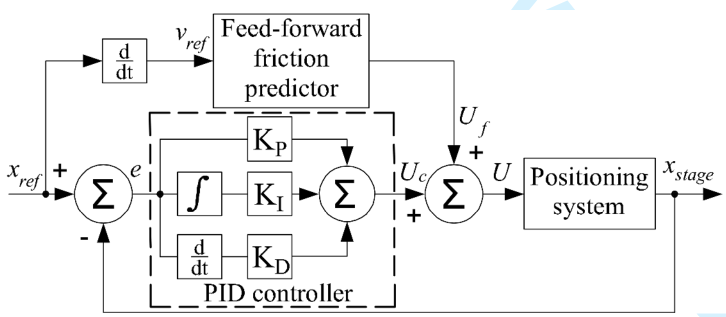

Fig. 8 Diagram of the controller based on feed-forward compensation of frictional disturbances comprising a simplified block diagram of the PID controller

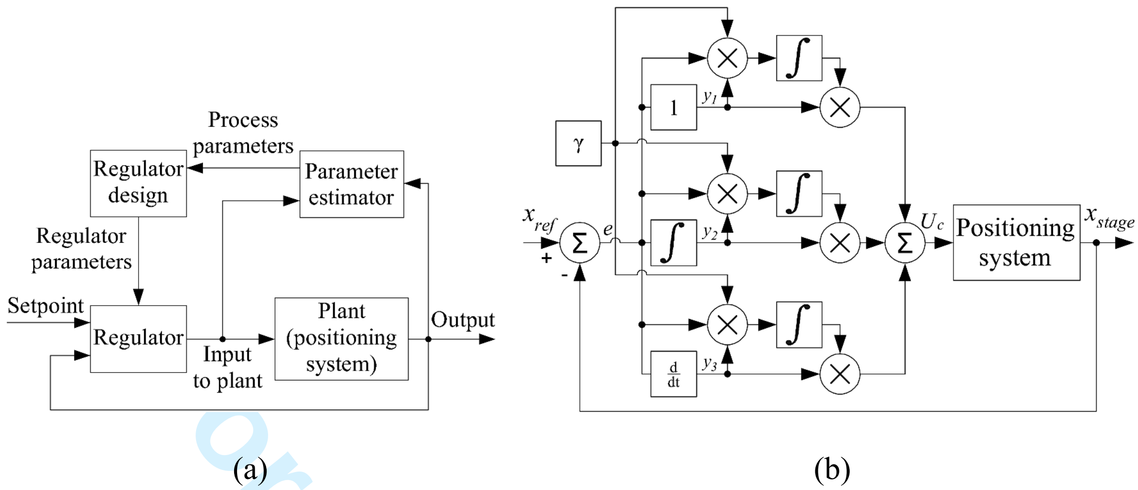

Fig. 9 Scheme of the STR adaptive controller (a) and STR adaptive PID controller structure (b)

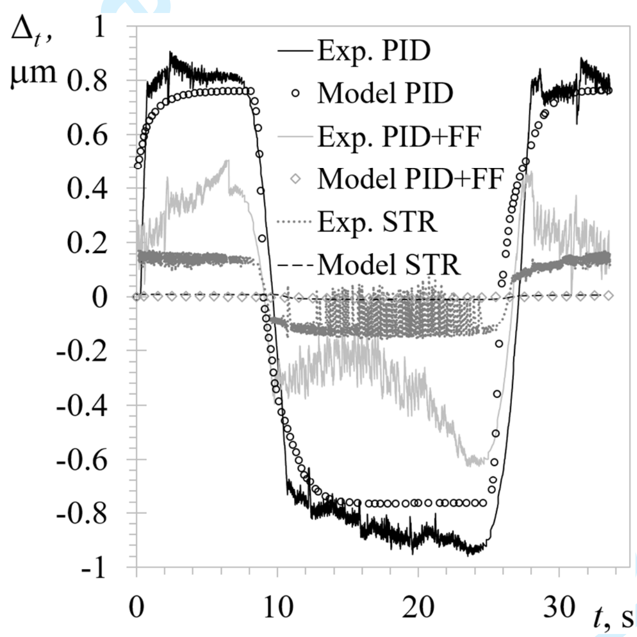

Fig. 10 Tracking errors Δ_t for sinusoidal 10 µm motions of the mechatronics device while employing the considered control typologies

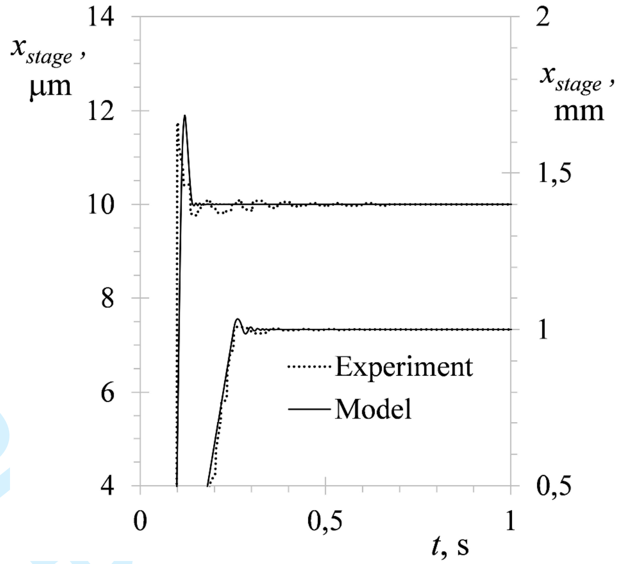

Fig. 11 Point-to-point positioning for short- and long-range motions

Table 1 Characteristic parameters of the Maxwell-slip blocks of the actuator-gearhead assembly

Maxwell-slip block no.	k_i, mNm/rad	α_i
1	1159	0.575
2	64.417	0.160
3	13.066	0.059
4	8.027	0.120
5	2.043	0.051
6	0.961	0.034

Table 2 Characteristic parameters of Stribeck curve of the actuator-gearhead assembly

Friction parameter	$\omega_r > 0$	$\omega_r < 0$	Nominal
M_s, µNm	219.3	218.6	219
M_C, µNm	120.4	130.8	125.6
ω_S, rad/s	0.14	0.23	0.18
δ	0.97	0.84	0.9
σ, µNm/rad·s^{-1}	10.33	10.69	10.51

Table 3 Characteristic parameters of the Maxwell-slip blocks of the linear guideways

Maxwell-slip block no.	k_i, N/m	α_i
1	454610	0.378
2	111088	0.138
3	45601	0.148
4	16402	0.177
5	6899	0.112
6	4295	0.046

Table 4 Accuracy and precision in repetitive point-to-point positioning with varying reference position values

x_{ref}, µm	Accuracy and precision, nm
1	173
10	160
100	219
1000	255